
Diffuse to Detect: Bi-Level Sample Rebalancing with Pseudo-Label Diffusion for Point-Supervised Infrared Small-Target Detection

Zhu Liu¹ Yuanhang Yao¹ Ping Qian¹ Zihang Chen¹ Risheng Liu¹

Abstract

Point supervision has become a scalable solution to address dense annotation for infrared small target detection, but its performance is limited by two coupled bottlenecks: unstable pseudo-label evolution in cluttered, low-contrast infrared imagery and severe sample-distribution imbalance. In this paper, we present a more adaptive and stable framework to address these issues. Leveraging the intrinsic consistency between thermal radiation patterns and heat diffusion, we propose a physics-induced annotation strategy that expands single-point labels into reliable pseudo-masks. To further enhance supervision and alleviate sample imbalance, we develop a bi-level dual-update framework that jointly optimizes detector weights, sample weights, and diffusion parameters. A meta-classifier dynamically predicts sample-wise loss weights, while a differentiable diffusion module refines pseudo-labels with detection feedback, enabling adaptive interaction between training and hyperparameter optimization. Extensive experiments across multiple datasets demonstrate five-fold annotation acceleration, superior detection accuracy, and comparable performance with 30% of the training data, validating the efficiency and practicality of our approach. Our code is available at <https://github.com/yuanhang-yao/diffuse-to-detect>.

1. Introduction

Infrared Small Target Detection (ISTD) is a long-standing and crucial task that aims to identify dim and tiny targets against cluttered backgrounds. As a component of infrared search-and-tracking systems, ISTD plays an indispensable

role in monitoring (Zhang et al., 2022b; Li et al., 2023b), navigation (Wang et al., 2025), early warning (Xu et al., 2023), and maritime resource management (Zhang et al., 2022a). However, due to the long-range imaging mechanism, targets are often shapeless and textureless, comprising only about 0.15% of the total pixels, making them easily overlooked within complex and noisy backgrounds, which further complicates detection.

Recently, data-driven learning paradigms (Dai et al., 2021a;b) have emerged as the mainstream solution, employing fully supervised pipelines to map infrared observations to pixel-level dense annotations. To capture discriminative features (Jiang et al., 2025a), existing methods design architectures guided by prior knowledge (Zhang et al., 2025a; Huang et al., 2025), including densely nested structures (Li et al., 2023b), vision transformers (Chen et al., 2024), or fine-tuning of large foundational models (Zhang et al., 2024b;a). Despite their promising performance, these approaches typically demand precise annotations and large-scale datasets covering diverse, high-stakes scenarios. We argue that the development of learning-based ISTD faces two major obstacles. First, most approaches rely on pixel-level dense annotations (Li et al., 2023a), which are costly to obtain and prone to errors due to the inherent characteristics of infrared small targets (*e.g.*, low Signal-to-Noise Ratio (SNR) and indistinct boundaries). Second, the scarcity of high-quality ISTD datasets (Liu et al., 2025c) leads to severe long-tailed distributions, as illustrated in Fig. 1 (a), *e.g.*, only 200 and 800 training pairs in SIRST-v1 and IRSTD-1k. Such imbalance hinders sufficient training on rare but critical cases, thereby limiting generalization.

Existing studies (Chen et al., 2014a; Gao et al., 2013) have explored single-point supervision as an alternative to alleviate the annotation burden. These approaches can be broadly divided into two promising directions. The first category employs online label updates. For example, LESPS (Ying et al., 2023) evolves pseudo-labels through intermediate indicators but suffers from excessive evolution and instability, while PAL (Yu et al., 2025a) integrates active learning with a coarse-to-fine training scheme to improve stability, yet still relies heavily on manual parameter tuning that limits its flexibility. In contrast, offline update strategies generate

¹School of Software Technology, Dalian University of Technology, Dalian, China. Correspondence to: Risheng Liu <rslu@dlut.edu.cn>.

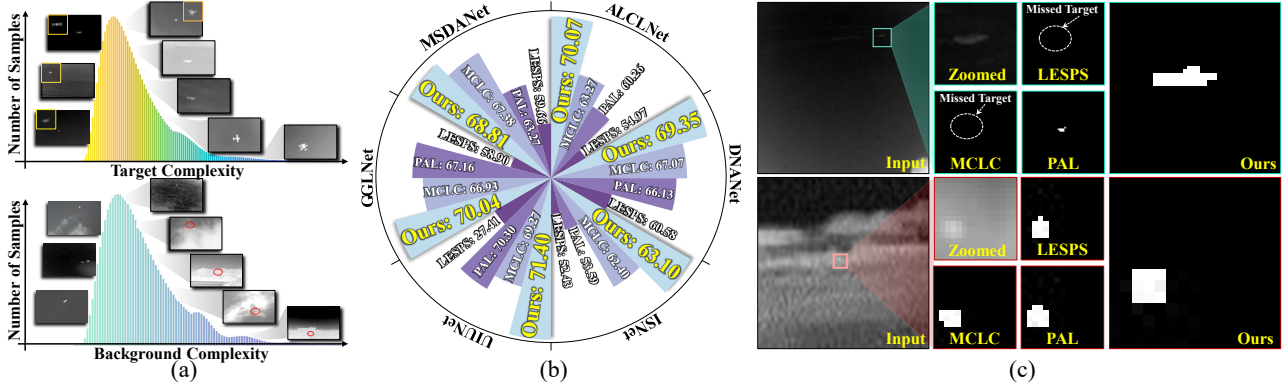


Figure 1. Motivation and efficiency overview. (a) Illustration of challenges including sample imbalance and complexity. (b) Quantitative results showing clear improvements using only 30% of the data. (c) Qualitative results validating our robustness in complex scenes.

pseudo-labels through dedicated algorithms (Li et al., 2023a; Kou et al., 2024), such as MCLC (Li et al., 2023a), which constructs labels from repeated noisy perturbations based on Monte Carlo linear clustering. However, these methods remain vulnerable to false positives, where background noise is mistakenly identified as targets. These limitations highlight the need for a more stable and precise automatic pseudo-label generation strategy.

Furthermore, several attempts have been made to alleviate the extreme sample imbalance in ISTD. Static loss reweighting schemes, such as focal loss (Xu et al., 2023), truncated squeeze loss (Zhang et al., 2025b) and adversarial learning (Wang et al., 2019) remain fixed throughout training. Curriculum-style methods, exemplified by progressive active learning, gradually introduce samples from easy to hard in a coarse-to-fine manner (Yu et al., 2025a), yet still rely on manually crafted schedules and heuristic criteria. Despite their merits, these approaches lack adaptability to the evolving training dynamics.

To address the aforementioned challenges, we propose a more adaptive and stable ISTD framework under single-point supervision. Leveraging the natural consistency between radiation patterns of infrared targets and physical heat diffusion, we first introduce an offline physics-induced annotation strategy that treats each spot as a thermal source, with diffusion governing the spatial spread of energy. To further refine supervision and reduce errors in complex cases, we develop a bi-level dual-update framework from the perspective of hyperparameter optimization. In this framework, the inner-level optimization updates the detector weights by minimizing the training loss, while the outer-level optimization adaptively adjusts two types of hyperparameters: sample weights and diffusion parameters. Specifically, a meta-classifier predicts sample-wise loss weights conditioned on training dynamics, enabling adaptive rebalancing of sample contributions. In parallel, the diffusion process is param-

eterized as a differentiable module, whose parameters are updated by the outer-level objective to ensure pseudo-labels evolve consistently with validation feedback. Furthermore, we design a dynamic aggregated solution to coordinate the interaction between model training and hyperparameter optimization. Extensive experiments demonstrate that our approach accelerates annotation by five times, achieves superior performance across multiple benchmarks, and attains comparable results using only 30% of the training data. The core contributions can be summarized as follows:

- We propose a bi-level dual-update optimization framework that jointly optimizes detector weights, sample weights, and annotation quality, achieving greater stability and adaptability than heuristic adjustments.
- By integrating a meta-classifier for sample-wise loss weighting with a differentiable diffusion module, our framework simultaneously rebalances samples and refines pseudo-labels under detection feedback.
- This work also introduces a physics-guided methodology for pseudo-mask generation, leveraging the intrinsic consistency between radiation patterns and heat diffusion to achieve efficient single-point supervision.
- Extensive experiments across multiple ISTD benchmarks validate the efficiency (annotation acceleration), effectiveness (superior detection accuracy), and practicality (fewer training samples) of our approach.

2. Related Work

SIRST detection has been widely studied for decades. Early research focused on model-driven traditional methods, including local contrast measurement methods (Chen et al., 2014a;b), filtering-based methods (Gao et al., 2013), and low-rank methods (He et al., 2015; Zhu et al., 2020).

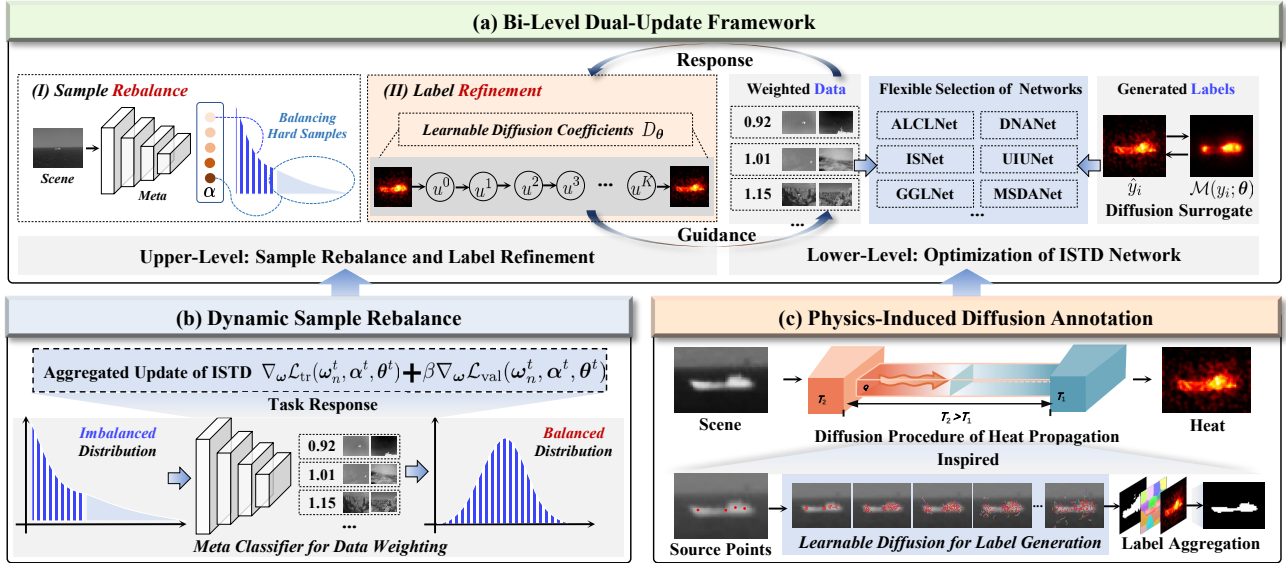


Figure 2. Overview of the proposed framework. (a) Bi-level dual-update framework performs joint sample rebalancing and label refinement. (b) Dynamic sample rebalancing is designed to weight training data. (c) Physics-induced diffusion annotation generates reliable pseudo-masks from single-point supervision in a learnable manner.

However, these methods require careful model design and fine-tuning of hyperparameters, resulting in poor adaptability and difficulty in dealing with complex and ever-changing real-world scenarios (Liu et al., 2023b). The subsequent emergence of deep learning methods (Zhao et al., 2022; Chen et al., 2023), especially fully supervised methods (Lu et al., 2024) based on customized architectures, has enabled models to learn the nonlinear mapping between input images (Zhao et al., 2022) and labels in a data-driven manner (Liu et al., 2024a). Various mechanisms including context aggregation (Lu et al., 2025), edge-guidance (Li et al., 2024b), dense feature representation (Li et al., 2023b), and spatial-frequency interaction, have been proposed (Liu et al., 2025b). Recently, several works have introduced granularity-aware modules and textual prompts into visual foundation models (e.g., SAM (Kirillov et al., 2023)). Unfortunately, these methods are limited by the scarcity of large-scale datasets, which limits generalization.

Point-based supervision has been proposed for diverse visual perception tasks, such as object detection (Ying et al., 2023), localization (Li et al., 2023b), and segmentation. For instance, in oriented object detection, WhollyWOOD (Yu et al., 2025c) studies unified weakly supervised oriented object detection with Point/HBox/RBox annotations, PointOBB (Luo et al., 2024) focuses on recovering object scale and angle from point supervision for oriented detection, and Point2RBox-v2 (Yu et al., 2025b) improves point-supervised oriented detection by modeling spatial layout among instances. At present, point-level segmentation methods require general targets with rich colors (Gao

et al., 2013), fine textures, and multiple annotated points, which pose challenges for the ISTD task. Ying et al. (Ying et al., 2023) proposed the LESPS framework that implements single-point supervised SIRST detection. However, the LESPS framework has issues such as instability and excessive label evolution. Li et al. (Li et al., 2023a) transformed fully supervised SIRST detection into a weakly supervised network with single-point supervision using the Monte Carlo clustering method, achieving remarkable performance while reducing annotation burden. Yu et al. (Yu et al., 2025a) proposed the PAL framework, which enables the initial selection of simple samples and the generation of corresponding pseudo-labels, effectively alleviating the problem of excessive label evolution. However, it lacks adaptability to the constantly evolving training dynamics and still requires adjustments. Thus, we aim to construct an efficient and adaptable framework.

3. The Proposed Method

3.1. Bi-Level Dual-Update Framework

In point-supervised ISTD, learning is fundamentally constrained by two coupled bottlenecks, including unstable pseudo-label evolution and severe sample-distribution imbalance. Importantly, the foundational issues amplify each other: imbalance makes the model more susceptible to overfitting to spurious background patterns in pseudo-labels, while noisy pseudo-labels further corrupt the estimation of sample importance, destabilizing the training dynamics. To overcome these issues, we introduce a bi-level dual-update

framework that jointly optimizes sample balance and supervision evolution based on the combination of offline and online updates, as shown in Fig. 2 (a). Hyperparameter optimization provides an effective tool for adaptively refining supervision according to model feedback, while the hierarchical separation enhances optimization stability and prevents error accumulation from noisy labels. Thus, we define the bi-level formulation (Liu et al., 2024c;b) as:

$$\begin{aligned} \min_{\alpha, \theta} \mathcal{L}_{\text{val}}(\omega^*(\alpha, \theta), \alpha, \theta) \\ \text{s.t. } \omega^*(\alpha, \theta) = \arg \min_{\omega} \sum_i \alpha_i \mathcal{L}_{\text{tr}}(\mathcal{N}(x_i; \omega), \hat{y}_i), \end{aligned} \quad (1)$$

where \mathcal{N} denotes the detector with parameters ω , and x_i and $\hat{y}_i(\theta)$ denote the input infrared image and its physics-induced pseudo-label, respectively. The variables α and θ correspond to two parallel hyperparameter branches in our framework. Specifically, the inner-level problem updates the detector parameters ω by minimizing the weighted training loss, where θ controls the diffusion-based annotation process and α denotes the sample-wise loss weights. The outer-level objective then refines both α and θ by minimizing the validation loss \mathcal{L}_{val} , which reflects how well the detector generalizes under the current supervision (Fig. 2 (b)). Note that, instead of leveraging real labels, we leverage the physics-induced pseudo-labels for the validation set. Compared with existing single-point supervised methods, the proposed bi-level dual-update framework establishes a dynamic closed-loop between model training and supervision generation, enabling continuous feedback to correct noisy labels and prevent overfitting.

3.2. Physics-Induced Diffusion Annotation

Infrared small targets are characterized by localized thermal emissions, small spatial size, and low signal-to-noise ratio (SNR). Most existing label-generation approaches often neglect the underlying physics of thermal propagation, failing to capture the spatial energy distribution. Physically, an infrared target acts as a local heat source, radiating energy that diffuses outward (Liu et al., 2016; Metzger et al., 2023). This diffusion is intrinsically governed by the local thermal conductivity of the surrounding medium (*e.g.*, texture and material), causing the energy to attenuate (Borgnakke & Sonntag, 2020). This motivates our formulation of pseudo-label generation as a learnable thermal diffusion process. We model the pseudo-label \hat{y}_i for the i -th target, identified by its single-point annotation p_i , as the quasi-steady thermal potential field $u(a, b)$ resulting from energy diffusion from the source p_i . The spatio-temporal evolution of this field, $u(a, b, t)$, is governed by a learnable anisotropic diffusion equation (Bao et al., 2023; Wang et al., 2023):

$$\frac{\partial u(a, b, t)}{\partial t} = \nabla \cdot (D_{\theta}(a, b) \nabla u(a, b, t)), \quad (2)$$

with the initial condition $u(a, b, 0) = \delta(a - p_i, b - p_i)$. Here, $D_{\theta}(a, b)$ is the spatially varying diffusion tensor with learnable parameters θ . It governs the local thermal conductivity and modulates the diffusion rate according to regional texture and contrast: propagation accelerates in homogeneous areas (to fill missing regions) while decelerating near edges and high-gradient structures (to prevent boundary smearing). For computational tractability, we discretize Eq. (2) into an iterative form:

$$u^{(k+1)} = (I - \tau L_{D_{\theta}})u^{(k)}, \quad u^{(0)} = \delta_{p_i}, \quad (3)$$

where $u^{(k)}$ is the thermal potential after the k -th iteration, τ is the diffusion step size, and $L_{D_{\theta}}$ is an image-adaptive Laplacian operator constructed from $D_{\theta}(a, b)$. After K iterations, $u^{(K)}$ represents the quasi-steady thermal field.

To enhance structural integrity and robustness, we aggregate this physics-based field with a data-driven spatial prior. Specifically, we introduce a superpixel segment $C_{p_i}(a, b)$, which is the binary mask of the superpixel region containing the annotation p_i . This prior provides a compact, data-driven boundary based on local image statistics. We then define the final pseudo-label \hat{y}_i as a learnable aggregation of these two information sources:

$$\hat{y}_i(\theta) = \rho \cdot u^{(K)}(a, b) + (1 - \rho) \cdot C_{p_i}(a, b), \quad (4)$$

where $\rho \in [0, 1]$ is a learnable balance parameter. This fusion adaptively controls the trade-off between the physics-informed diffusion $u^{(K)}$ and the compact structural prior C_{p_i} . The aggregated field $\hat{y}_i(\theta)$ is subsequently normalized to $[0, 1]$. The final pseudo-label $\hat{y}_i(\theta)$ thus preserves both physical continuity and structural precision, serving as a differentiable supervision signal for the bi-level optimization framework, as shown in Fig. 2 (c).

3.3. Dynamic Aggregated Solution

In practice, solving the hyperparameter optimization in Eq. (1) is computationally demanding, as it typically requires high-order unrolled gradients (Liu et al., 2025a) or implicit differentiation (Liu et al., 2022). Although alternating updates can reduce computational burden, they often lead to unstable convergence due to the mismatched update frequencies between the inner and outer levels. To overcome these limitations, we introduce a first-order dynamic aggregated solution (Liu et al., 2023a) that enables efficient and coherent interaction between model parameters and hyperparameters within a unified optimization.

Inspired by recent work on single-loop bi-level optimization (Jiang et al., 2025b), we dynamically combine these two objectives to update the model parameters in the inner loop to obtain ω^{t+1} : $\omega_{n+1}^t = \omega_n^t - \left(\nabla_{\omega} \mathcal{L}_{\text{tr}}(\omega_n^t, \alpha^t, \theta^t) + \beta \nabla_{\omega} \mathcal{L}_{\text{val}}(\omega_n^t, \alpha^t, \theta^t) \right)$, where β controls how strongly the

Table 1. Performance of ISTD under different training strategies. All models are trained on SIRST3 and evaluated on SIRST3 and three individual datasets (SIRST-v1, NUDT-SIRST, IRSTD-1k). We report four metrics: IoU (%), nIoU (%), P_d (%), and F_a (10^{-6}).

Scheme	Description	SIRST3				SIRST-v1				NUDT-SIRST				IRSTD-1k			
		IoU \uparrow	nIoU \uparrow	$P_d\uparrow$	$F_a\downarrow$	IoU \uparrow	nIoU \uparrow	$P_d\uparrow$	$F_a\downarrow$	IoU \uparrow	nIoU \uparrow	$P_d\uparrow$	$F_a\downarrow$	IoU \uparrow	nIoU \uparrow	$P_d\uparrow$	$F_a\downarrow$
MLCLNet (Yu et al., 2022a)	Full	81.04	83.56	95.95	14.07	69.01	75.37	92.78	62.56	91.25	91.54	97.67	10.09	64.29	64.22	92.93	7.91
	LESPTS	35.02	44.81	69.50	28.22	44.93	52.68	77.95	33.79	38.71	46.31	70.16	27.16	26.75	41.49	71.04	22.75
	PAL	64.17	68.48	94.85	18.26	63.48	68.41	92.02	22.43	66.68	72.12	96.88	22.09	63.11	56.34	89.24	17.63
	MCLC	65.16	67.95	96.22	30.53	64.83	68.17	89.92	40.41	68.51	71.23	94.07	31.80	55.44	56.30	87.58	14.90
	Ours	69.95	72.61	94.57	11.12	65.70	69.39	92.59	7.90	78.68	85.70	97.67	12.79	60.19	56.94	90.12	11.20
ALCLNet (Yu et al., 2022b)	Full	82.12	82.57	96.15	13.36	75.65	75.91	96.20	24.90	88.78	89.26	97.67	10.23	65.87	64.31	91.25	12.13
	LESPTS	30.59	43.91	70.30	34.36	42.61	53.35	76.81	37.65	31.33	43.47	70.26	37.87	25.61	42.18	71.04	27.27
	PAL	60.26	64.67	91.89	35.34	64.19	68.99	92.78	30.80	63.67	65.98	93.12	40.84	42.86	54.08	86.63	26.14
	MCLC	63.27	65.70	91.89	47.19	68.09	72.41	93.54	51.86	63.01	65.58	91.22	49.25	58.15	55.94	88.26	34.47
	Ours	73.28	73.30	95.44	16.35	74.34	72.92	98.15	13.82	79.94	85.50	97.67	10.04	63.96	57.66	92.18	24.29
DNANet (Li et al., 2023b)	Full	85.49	86.22	96.88	8.14	77.95	80.35	96.58	22.23	93.90	94.06	98.84	3.06	65.21	66.64	91.25	10.21
	LESPTS	36.98	47.59	86.84	28.97	44.39	52.49	84.79	30.10	37.27	46.40	90.58	26.04	31.97	47.92	76.43	27.80
	PAL	66.13	70.37	94.76	21.38	67.28	70.91	95.06	22.09	71.23	73.53	96.88	22.24	48.89	57.38	89.27	23.85
	MCLC	67.07	69.29	94.22	33.03	68.08	69.08	95.96	37.32	70.22	73.03	94.71	35.46	56.92	56.66	90.57	23.55
	Ours	71.08	74.65	95.24	15.16	68.27	73.49	96.30	14.90	79.99	87.01	97.67	13.65	61.38	58.07	90.82	17.00
ISNet (Zhang et al., 2022b)	Full	74.38	76.34	93.29	28.10	70.47	72.89	92.78	41.23	80.19	81.73	94.18	22.41	61.46	60.52	89.23	32.13
	LESPTS	32.22	44.20	77.94	36.98	40.71	51.00	82.13	38.59	35.46	45.63	79.15	35.02	24.02	38.40	71.72	36.74
	PAL	53.59	58.42	86.11	35.57	53.01	60.53	88.21	32.38	57.69	62.15	88.68	34.75	31.92	45.23	77.78	39.89
	MCLC	62.40	64.07	90.42	45.53	65.12	68.04	94.68	27.71	65.13	66.88	92.76	55.59	52.65	52.35	85.58	32.57
	Ours	65.83	69.39	91.02	19.29	66.82	71.14	96.30	23.21	72.60	79.91	93.02	9.24	54.81	53.53	86.39	30.59
UIUNet (Wu et al., 2023)	Full	85.21	85.73	97.01	11.86	76.74	78.53	95.82	21.82	93.57	93.75	98.62	4.69	68.22	66.57	93.27	20.95
	LESPTS	39.38	50.20	75.81	33.43	53.06	60.58	82.89	29.76	40.17	49.04	75.24	30.32	32.37	47.56	76.09	36.25
	PAL	70.30	71.95	94.48	25.29	72.15	74.15	95.44	34.64	71.95	73.71	97.31	20.87	65.82	62.21	91.95	31.35
	MCLC	69.27	71.07	94.81	37.60	72.45	73.76	96.20	42.26	69.81	73.35	96.08	36.97	65.15	63.79	91.93	36.31
	Ours	73.65	75.60	96.31	15.40	73.00	74.59	100.00	11.49	79.33	84.22	97.67	15.95	65.86	64.75	92.16	16.93
GGLNet (Zhao et al., 2023)	Full	84.08	85.38	97.61	8.58	78.82	79.45	97.34	25.93	92.33	92.86	99.26	3.65	64.52	65.54	91.58	8.27
	LESPTS	40.89	50.95	74.42	33.34	50.07	59.07	79.85	33.94	43.61	51.04	76.19	37.03	32.26	46.75	71.04	28.67
	PAL	67.16	70.42	94.95	27.19	68.81	71.78	96.20	27.51	71.07	72.71	97.46	26.93	53.08	59.54	89.23	27.19
	MCLC	66.93	68.64	93.15	26.02	70.20	71.94	97.72	21.40	68.24	70.26	93.23	26.34	56.82	58.87	88.92	29.98
	Ours	71.73	75.35	95.04	16.23	72.55	73.37	98.15	11.13	82.20	88.33	98.26	14.63	58.24	59.91	89.80	20.48
MSDANet (Zhao et al., 2025)	Full	86.16	86.13	97.01	11.04	76.40	78.03	94.30	25.79	94.01	94.18	98.73	1.47	71.64	68.09	93.94	28.26
	LESPTS	39.03	49.84	82.86	25.58	50.27	58.15	85.17	22.43	39.60	48.67	84.23	24.82	33.11	47.70	78.11	29.42
	PAL	63.27	68.68	94.15	23.29	67.76	71.34	94.68	16.81	67.48	70.61	96.83	23.76	47.80	58.02	89.23	27.54
	MCLC	67.38	69.88	93.82	37.35	70.61	72.31	96.96	14.13	68.94	71.67	94.81	47.68	58.84	58.71	89.93	27.33
	Ours	71.41	73.16	94.37	12.71	71.99	72.51	97.22	7.54	79.25	85.38	97.09	5.85	60.61	59.38	90.82	23.76

outer-level objective influences the inner-level parameter updates, achieving a balance between leveraging validation feedback and maintaining training stability. This dynamic aggregation allows the model parameters to evolve under both task-specific supervision and meta-level feedback. Subsequently, the hyperparameters α are updated in a one-step gradient manner based on the latest model parameters ω^{t+1} : $\alpha^{t+1} = \alpha^t - \nabla_{\alpha} \mathcal{L}_{\text{val}}(\omega^{t+1}, \alpha^t, \theta^t)$. This update strategy ensures that the learned loss weights are adaptively aligned with the outer-level objectives. Finally, we refine the diffusion parameters θ by aligning the differentiable diffusion surrogate \mathcal{M} with the physics-induced pseudo-labels produced by the offline annotator. Given the detector prediction $y_i = \mathcal{N}(x_i; \omega)$, the surrogate diffusion module outputs a soft mask $\mathcal{M}(y_i; \theta)$, while \hat{y}_i denotes the corresponding pseudo-label generated by the basic physics-induced diffusion process. We update θ with a single gradient step: $\theta^{t+1} = \theta^t - \nabla_{\theta} (\mathcal{L}_{\text{val}}(\mathcal{M}(y_i; \theta), \hat{y}_i) + \mathcal{L}_{\text{val}}(\mathcal{M}(y_i; \theta), y_i))$. Here, the first term encourages \mathcal{M} to reproduce the physics-induced pseudo-labels, while the second term regularizes the update by keeping $\mathcal{M}(y_i; \theta)$ consistent with the current response, mitigating overfitting to potentially noisy supervision. This design ensures that the

outer objective provides a stable signal for generalization-oriented weighting and hyperparameter calibration, while preventing the validation loss from collapsing into self-consistency with the current predictions.

4. Experiments

4.1. Implementation Configurations

Datasets. We evaluate on four representative datasets: SIRST3 (Ying et al., 2023), SIRST-v1 (Dai et al., 2021a), NUDT-SIRST (Li et al., 2023b), and IRSTD-1k (Zhang et al., 2022b), which contain 2,755, 427, 1,327, and 1,001 samples, respectively. Since there is no common practice of using a validation set on these benchmarks, we adopt a 6:2:2 partition for each of SIRST-v1, NUDT-SIRST, and IRSTD-1k, following the official splitting protocols (Dai et al., 2021a; Li et al., 2023b; Zhang et al., 2022b). For SIRST3, we merge the three subsets and perform a 6:2:2 split for train/val/test to evaluate robustness on diverse scenes.

Experimental settings. We trained for 400 epochs using the AdamW optimizer with a batch size of 16 and a learning rate of 1×10^{-3} . Outer-level update activates at epoch 80, updating the sample-weighting and pseudo-label branches in

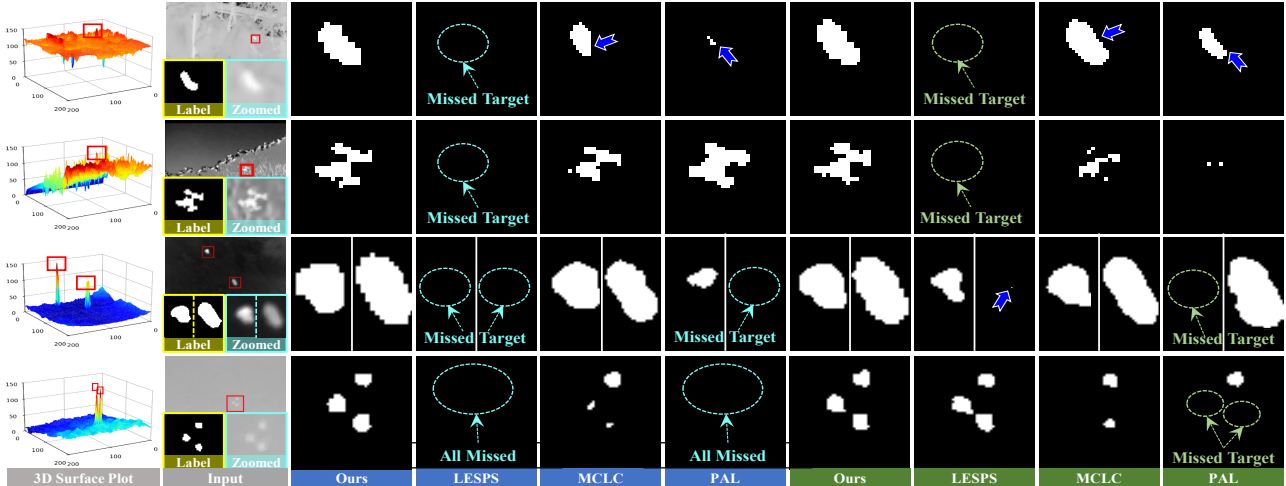


Figure 3. Qualitative comparison on the SIRST3 dataset. Columns from left to right: 3D surfaces of inputs, input images with labels and local magnification, Ours, LESPS, MCLC, and PAL predictions (the blue part on ALCLNet, the green part on DNANet).

Table 2. Performance of ISTD under different training strategies. Models are trained on three individual datasets (SIRST-v1, NUDT-SIRST, IRSTD-1k). We report four metrics: IoU (%), nIoU (%), P_d (%), and F_a (10^{-6}).

Methods	Strategy	SIRST-v1				NUDT-SIRST				IRSTD-1k			
		IoU \uparrow	nIoU \uparrow	$P_d\uparrow$	$F_a\downarrow$	IoU \uparrow	nIoU \uparrow	$P_d\uparrow$	$F_a\downarrow$	IoU \uparrow	nIoU \uparrow	$P_d\uparrow$	$F_a\downarrow$
ALCLNet (Yu et al., 2022b)	Full	72.57	72.66	94.68	30.39	89.79	89.95	98.84	6.69	65.23	64.25	89.90	9.19
	LESPS	39.85	43.16	73.76	35.37	36.76	44.90	73.02	39.02	33.73	47.75	80.81	36.21
	PAL	60.49	62.48	86.69	43.63	67.40	68.89	96.61	23.00	57.48	55.40	87.54	27.86
	MCLC	71.80	71.71	95.06	33.07	68.89	70.84	95.45	39.94	63.11	59.66	91.58	29.80
	Ours	75.62	71.93	98.15	2.51	79.88	85.50	96.80	17.27	64.72	60.35	92.52	18.07
DNANet (Li et al., 2023b)	Full	77.55	77.76	94.30	11.66	95.35	95.43	99.26	2.00	67.74	63.66	88.55	17.56
	LESPS	54.39	61.13	89.35	30.18	36.98	46.46	66.14	31.97	30.59	47.47	72.39	29.60
	PAL	64.83	65.94	92.78	30.87	70.70	71.34	97.78	24.57	62.29	58.46	87.88	20.65
	MCLC	69.61	72.21	96.96	24.08	70.86	72.82	96.19	25.00	61.79	64.32	90.91	32.51
	Ours	75.49	72.94	99.07	8.08	79.32	87.20	98.26	10.21	63.64	64.67	92.59	18.67
UIUNet (Wu et al., 2023)	Full	80.03	78.99	94.68	9.12	95.38	95.22	99.05	1.38	70.36	64.09	93.60	18.24
	LESPS	46.82	55.18	78.71	26.40	39.63	46.56	68.04	20.04	39.90	49.67	80.47	20.70
	PAL	63.98	62.39	92.02	28.95	70.81	72.43	98.20	13.42	57.50	56.98	89.90	11.86
	MCLC	71.01	68.87	90.11	22.91	70.20	72.22	94.71	21.46	66.19	62.31	88.89	39.30
	Ours	71.85	69.55	99.07	11.31	79.84	85.19	98.55	6.77	68.19	62.86	90.14	6.07
MSDANet (Zhao et al., 2025)	Full	75.82	76.49	95.06	38.49	95.65	95.48	99.47	1.38	68.08	64.29	91.92	24.05
	LESPS	48.69	55.86	82.89	32.12	36.34	45.45	73.76	19.40	38.73	49.79	81.48	33.55
	PAL	63.27	66.92	93.92	29.64	59.46	63.76	93.54	16.13	59.52	58.16	89.90	26.94
	MCLC	71.23	72.35	92.02	31.83	69.67	71.61	94.92	26.52	62.83	61.77	87.54	32.32
	Ours	76.33	73.79	100.00	3.77	79.08	86.05	98.84	13.19	63.31	62.94	90.12	25.98

parallel. The pseudo-label branch updates every 20 epochs via a separate Adam optimizer with learning rate 1×10^{-2} . Inputs were normalized and randomly cropped to 256×256 . Soft IoU loss is used to define \mathcal{L}_{val} and \mathcal{L}_{tr} . Both the training and validation sets are supervised only by single-point annotations, and all image priors used in our method are computed solely from the input infrared images. We report standard SIRST metrics (IoU, nIoU, P_d , F_a) to assess segmentation fidelity, missed targets, and false positives.

4.2. Experimental Results

Evaluation on the SIRST3 dataset. Table 1 presents a comprehensive performance comparison of our proposed training strategy against leading single-point supervision baselines (LESPS, PAL, MCLC) and a fully supervised

(Full) upper bound. The evaluation spans seven different detector architectures on the comprehensive SIRST3 benchmark. The results definitively demonstrate that our approach consistently and significantly outperforms all competing single-point supervision methods across nearly every metric and detector. This trend of superiority is consistent across all benchmarks; on SIRST3, our strategy achieves the highest IoU and nIoU for every evaluated detector among all non-full supervision methods.

Fig. 3 provides a detailed qualitative comparison of our method against typical single-point supervision baselines (LESPS, MCLC, and PAL) on challenging examples from the SIRST3 dataset. The analysis highlights a clear pattern of robustness for our approach. In high-clutter environments where targets are adjacent to bright edges or complex struc-

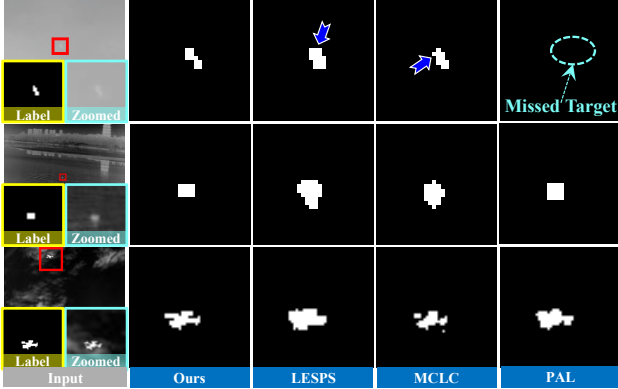


Figure 4. Qualitative comparison on three representative scenes. These results are obtained by ALCLNet.

tures (Rows 1 and 2), competing methods struggle significantly. A multi-target case is shown in the third row, where our method separates targets cleanly and avoids merging them into surrounding structures, while preserving target boundaries more effectively overall. A low-contrast multi-target scenario is shown in the last row, where our method achieves higher detection accuracy by successfully identifying faint targets that other methods often miss.

Evaluation on three individual datasets. We validated our framework’s stability and robustness both qualitatively (Fig. 4) and quantitatively (Table 2) on individual datasets. In challenging high-clutter and low-SNR scenes, our method reliably localizes targets while suppressing noise. In contrast, baselines like LESPS, MCLC, and PAL suffer from unstable evolution, missed detections, and false alarms. This stability is quantitatively confirmed on scarce-data benchmarks, where our method consistently and significantly outperforms all competitors; for example, achieving over 20 percentage points of IoU improvement over LESPS.

4.3. Ablation Studies

Efficiency of the proposed framework. Table 3 presents an ablation analysis of the core components of our framework on SIRST3. Two obvious conclusions can be obtained. First, supervision quality is the primary bottleneck: Combining diffusion with the superpixel prior improves all metrics, suggesting complementary effects of diffusion expanding supervision, while the superpixel prior regularizes boundaries and suppresses label noise. Second, the training strategy is essential for turning better pseudo-labels into stable optimization: removing the bi-level dual-update, balance, online label update, or dynamic aggregation (B1-B4) consistently degrades performance. Overall, these results support that effective pseudo-label construction and stable bi-level optimization are both necessary, and their combination leads to the best performance.

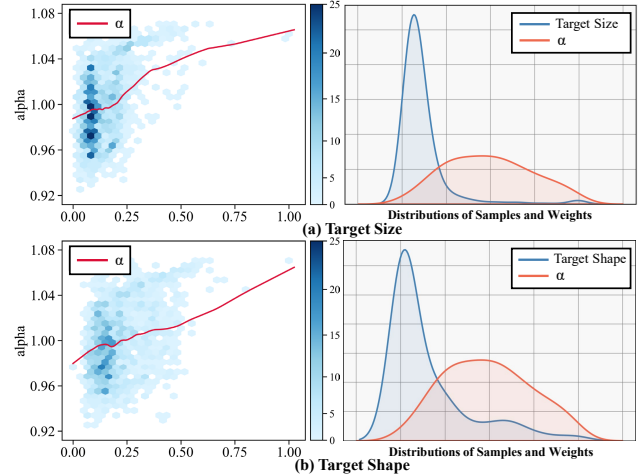


Figure 5. Analysis of the learned sample weight α . The left plot shows the correlation of α with target size (small to large diameter) and target shape (near-circular to irregular), while the right plot shows the distribution of target shape, target size and α .

Table 3. Ablation of core components in our framework. These results are obtained by ALCLNet.

Model Variants	SIRST3		
	IoU \uparrow	nIoU \uparrow	P α \uparrow
(A1) Naive point supervision	8.07	17.51	78.02
(A2) Diffusion only	69.64	70.80	91.82
(A3) Superpixel prior only	68.64	69.41	93.16
(A4) Diffusion + Superpixel (numerical)	70.75	71.47	94.50
(B1) Direct joint learning	67.10	69.49	89.54
(B2) w/o balance ($\alpha \equiv 1$)	70.96	72.95	94.24
(B3) w/o online label update	71.52	71.26	93.43
(B4) w/o dynamic aggregation ($\beta = 0$)	67.74	68.60	92.23
Proposed	73.28	73.30	95.44

Verification of sample rebalancing. To validate the meta-network’s learned behavior, we conducted a statistical analysis of the weights α_i aggregated over 100 runs. As illustrated in Fig. 5, the weights correlate strongly with sample difficulty: challenging samples (e.g., larger, irregular targets) receive higher α_i , while easy samples (e.g., small, compact targets) are assigned lower weights. Crucially, the weight density appears inversely correlated with the sample density; regions with high α density are precisely those where the sample density is low. The weighting branch automatically compensates for under-represented but challenging cases by upweighting them, while downweighting abundant cases.

Validation of data usage. We found that the learned weights α_i can also be used to guide data selection, reducing annotation and training costs. Experiments demonstrate that a standard detector trained from scratch using only the top 30% of the sample subset, selected via α_i ranking, already surpasses the performance of baselines trained on 100% of the data, as shown in Fig. 6. This indicates that our bi-level optimization framework can effectively identify informative samples and safely discard redundant data. Fig. 7 (a)

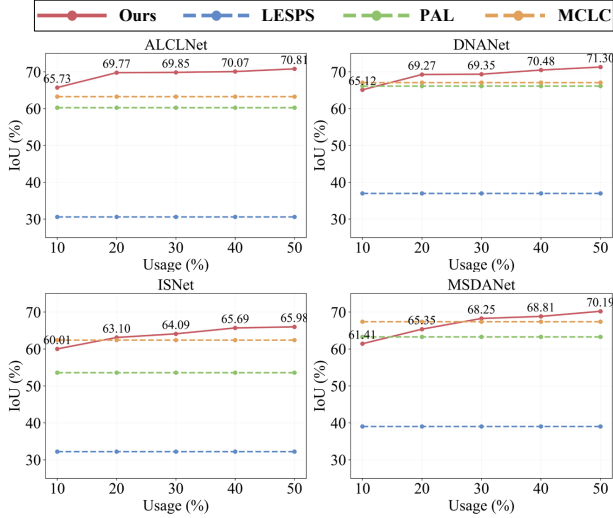


Figure 6. Data-efficiency on SIRST3 dataset across diverse networks, comparing Ours, LESPS, PAL, and MCLC under single-point supervision. Others are trained with full training datasets.

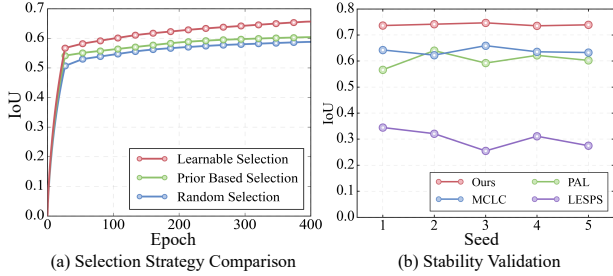


Figure 7. Convergence of sample-selection strategy and stability validation on SIRST3 under diverse seeds.

compares three data selection strategies under the same data budget. Our learned weights clearly outperform random and prior-based (hand-crafted difficulty) selection, showing more reliable identification of informative samples. Fig. 7 (b) reports results under five random seeds. Our method exhibits smaller variance than the baselines, demonstrating significantly improved training stability.

Time efficiency of diffusion annotation. We evaluated our proposed physics-induced diffusion annotation against existing single-point methods (COM and MCLC) in terms of both quality and efficiency. Moreover, as shown in Table 4, our pseudo-masks achieve an IoU of up to 68.02 against ground truth on the SIRST3 dataset, outperforming MCLC (66.98) and COM (15.62). As shown in Fig. 8, visual comparisons also confirm that while COM tends to under-segment and MCLC often over-grows into the background, our method better maintains clean target boundaries. In terms of efficiency, our method requires only 0.012 seconds per target on a CPU, which is approximately five times faster than MCLC (0.069s) and nearly two orders of magnitude faster than COM (0.923s). This high efficiency (a five-fold

Table 4. Pseudo-mask generation on four ISTD datasets with Centroid and Coarse initialization, comparing COM, MCLC, and Ours, and reporting IoU and average time per target.

Centroid	SIRST3	SIRST-v1	NUDT-SIRST	IRSTD-1k	Average Time↓
	IoU↑	IoU↑	IoU↑	IoU↑	
COM (Li et al., 2024a)	15.62	21.72	7.80	36.86	0.923s
MCLC (Li et al., 2023a)	66.98	75.50	62.97	68.65	0.069s
Ours	68.02	74.58	64.48	70.12	0.012s
Coarse	SIRST3	SIRST-v1	NUDT-SIRST	IRSTD-1k	Average Time↓
	IoU↑	IoU↑	IoU↑	IoU↑	
COM (Li et al., 2024a)	15.01	20.76	7.67	35.11	0.961s
MCLC (Li et al., 2023a)	63.71	74.19	58.47	66.18	0.069s
Ours	65.69	73.78	59.15	68.42	0.013s

Table 5. Pseudo-mask generation on four ISTD datasets with Centroid and Coarse initialization, comparing SAM, SAM2, and Ours, reporting IoU and average time per target.

Centroid	SIRST3	SIRST-v1	NUDT-SIRST	IRSTD-1k	Average Time↓
	IoU↑	IoU↑	IoU↑	IoU↑	
SAM (Kirillov et al., 2023)	44.98	55.39	41.54	45.41	0.105s
SAM2 (Ravi et al., 2025)	47.39	57.01	47.91	43.31	0.156s
Ours	68.02	74.58	64.48	70.12	0.012s
Coarse	SIRST3	SIRST-v1	NUDT-SIRST	IRSTD-1k	Average Time↓
	IoU↑	IoU↑	IoU↑	IoU↑	
SAM (Kirillov et al., 2023)	6.03	4.41	7.98	4.13	0.135s
SAM2 (Ravi et al., 2025)	47.14	57.06	47.67	42.95	0.149s
Ours	65.69	73.78	59.15	68.42	0.013s

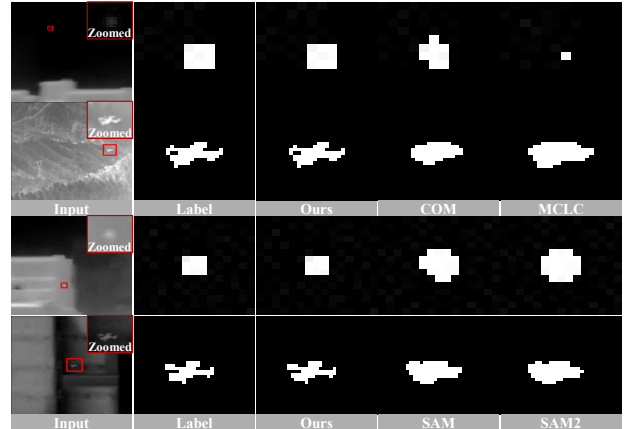


Figure 8. Qualitative comparison of small target detection on the SIRST3 dataset: Ours vs. COM, MCLC, SAM, and SAM2.

speedup over MCLC) is crucial: it makes the diffusion module lightweight enough to be embedded within the bi-level optimization loop. We compared our proposed physics-diffusion annotation with foundation models SAM/SAM2 in Table 5. Visually, SAM/SAM2 perform poorly on infrared small targets, often either missing them or causing severe over-segmentation, as shown in Fig. 8. In contrast, our method generates compact masks that better follow the target’s true thermal footprint. In terms of efficiency, our diffusion module is also significantly faster than SAM/SAM2. This demonstrates that for single-point supervised ISTD, a dedicated physics-guided framework remains superior to generic foundation models in both accuracy and efficiency.

5. Conclusion

In this paper, we proposed a bi-level dual-update framework built upon single-point supervision to address annotation costs and sample imbalance jointly. First, we introduced a physics-induced annotation strategy. Second, we addressed the joint optimization of the detector, sample importance weights, and annotation quality. Extensive experiments demonstrated that our approach is highly efficient, achieving superior detection accuracy.

Impact Statement

This paper presents work whose goal is to advance the field of Machine Learning. There are many potential societal consequences of our work, none which we feel must be specifically highlighted here.

Acknowledgements

This work is partially supported by the National Natural Science Foundation of China (Nos.U22B2052, 624B2033), Central Guidance for Local Science and Technology Development Fund (Youth Science Fund Project, Category A, No. 2025JH6/101100001), the Distinguished Young Scholars Funds of Dalian (No.2024RJ002), and the Fundamental Research Funds for the Central Universities.

References

- Bao, F., Wang, X., Sureshbabu, S. H., Sreekumar, G., Yang, L., Aggarwal, V., Boddeti, V. N., and Jacob, Z. Heat-assisted detection and ranging. *Nature*, 619(7971):743–748, 2023.
- Borgnakke, C. and Sonntag, R. E. *Fundamentals of thermodynamics*. John Wiley & Sons, 2020.
- Chen, C. L. P., Li, H., Wei, Y., Xia, T., and Tang, Y. Y. A local contrast method for small infrared target detection. *IEEE Transactions on Geoscience and Remote Sensing*, 52(1):574–581, 2014a.
- Chen, T., Chu, Q., Liu, B., and Yu, N. Fluid dynamics-inspired network for infrared small target detection. In *International Joint Conference on Artificial Intelligence*, pp. 590–598. IJCAI Press, 2023.
- Chen, T., Tan, Z., Chu, Q., Wu, Y., Liu, B., and Yu, N. TCI-Former: Thermal conduction-inspired transformer for infrared small target detection. In *Proceedings of the AAAI Conference on Artificial Intelligence*, volume 38, pp. 1201–1209. AAAI Press, 2024.
- Chen, Z., Luo, S., Xie, T., Liu, J., Wang, G., and Lei, G. A novel infrared small target detection method based on BEMD and local inverse entropy. *Infrared Physics & Technology*, 66:114–124, 2014b.
- Dai, Y., Wu, Y., Zhou, F., and Barnard, K. Asymmetric contextual modulation for infrared small target detection. In *Proceedings of the IEEE/CVF Winter Conference on Applications of Computer Vision*, pp. 950–959. IEEE, 2021a.
- Dai, Y., Wu, Y., Zhou, F., and Barnard, K. Attentional local contrast networks for infrared small target detection. *IEEE Transactions on Geoscience and Remote Sensing*, 59(11):9813–9824, 2021b.
- Gao, C., Meng, D., Yang, Y., Wang, Y., Zhou, X., and Hauptmann, A. G. Infrared patch-image model for small target detection in a single image. *IEEE Transactions on Image Processing*, 22(12):4996–5009, 2013.
- He, Y., Li, M., Zhang, J., and An, Q. Small infrared target detection based on low-rank and sparse representation. *Infrared Physics & Technology*, 68:98–109, 2015.
- Huang, F., Zheng, S., Qiu, Z., Liu, H., Bai, H., and Chen, L. Text-IRSTD: Leveraging semantic text to promote infrared small target detection in complex scenes. In *Proceedings of the IEEE/CVF International Conference on Computer Vision*, pp. 10635–10644. IEEE, October 2025.
- Jiang, C., Kilcullen, P., Lai, Y., Ozaki, T., and Liang, J. Single-pixel infrared imaging thermometry maps human inner canthi temperature. *Nature Communications*, 16(1):8885, 2025a.
- Jiang, L., Xiao, Q., Chen, L., and Chen, T. Beyond value functions: Single-loop bilevel optimization under flatness conditions. *Advances in Neural Information Processing Systems*, 38:52003–52040, 2025b.
- Kirillov, A., Mintun, E., Ravi, N., Mao, H., Rolland, C., Gustafson, L., Xiao, T., Whitehead, S., Berg, A. C., Lo, W. Y., Dollár, P., and Girshick, R. Segment anything. *arXiv preprint arXiv:2304.02643*, 2023.
- Kou, R., Wang, C., Fu, Q., Li, Z., Luo, Y., Li, B., Li, W., and Peng, Z. MCGC: A multiscale chain growth clustering algorithm for generating infrared small target mask under single-point supervision. *IEEE Transactions on Geoscience and Remote Sensing*, pp. 1–12, 2024.
- Li, B., Wang, Y., Wang, L., Zhang, F., Liu, T., Lin, Z., An, W., and Guo, Y. Monte Carlo linear clustering with single-point supervision is enough for infrared small target detection. In *Proceedings of the IEEE/CVF International Conference on Computer Vision*, pp. 1009–1019. IEEE, 2023a.

- Li, B., Xiao, C., Wang, L., Wang, Y., Lin, Z., Li, M., An, W., and Guo, Y. Dense nested attention network for infrared small target detection. *IEEE Transactions on Image Processing*, 32:1745–1758, 2023b.
- Li, H., Yang, J., Xu, Y., and Wang, R. A level set annotation framework with single-point supervision for infrared small target detection. *IEEE Signal Processing Letters*, 31:451–455, 2024a. doi: 10.1109/LSP.2024.3356411.
- Li, Q., Zhang, M., Yang, Z., Yuan, Y., and Wang, Q. Edge-guided perceptual network for infrared small target detection. *IEEE Transactions on Geoscience and Remote Sensing*, pp. 1–10, 2024b.
- Liu, Q., Liu, R., Zheng, B., Wang, H., and Fu, Y. Infrared small target detection with scale and location sensitivity. In *Proceedings of the IEEE/CVF Conference on Computer Vision and Pattern Recognition*, pp. 17490–17499. IEEE, 2024a.
- Liu, R., Zhong, G., Cao, J., Lin, Z., Shan, S., and Luo, Z. Learning to diffuse: A new perspective to design PDEs for visual analysis. *IEEE Transactions on Pattern Analysis and Machine Intelligence*, 38(12):2457–2471, 2016.
- Liu, R., Gao, J., Zhang, J., Meng, D., and Lin, Z. Investigating bi-level optimization for learning and vision from a unified perspective: A survey and beyond. *IEEE Transactions on Pattern Analysis and Machine Intelligence*, 44(12):10045–10067, 2022.
- Liu, R., Liu, Z., Liu, J., Fan, X., and Luo, Z. A task-guided, implicitly-searched and meta-initialized deep model for image fusion. *IEEE Transactions on Pattern Analysis and Machine Intelligence*, 46(10):6594–6609, 2024b.
- Liu, R., Liu, Z., Yao, W., Zeng, S., and Zhang, J. Moreau envelope for nonconvex bi-level optimization: a single-loop and hessian-free solution strategy. In *Proceedings of the 41st International Conference on Machine Learning*, pp. 31566–31596. PMLR, 2024c.
- Liu, R., Liu, Z., Mao, W., Yao, W., and Zhang, J. Bilevel optimization for adversarial learning problems: Sharpness, generation, and beyond. *Advances in Neural Information Processing Systems*, 38:29102–29130, 2025a.
- Liu, Y., Tu, B., Liu, B., He, Y., Li, J., and Plaza, A. Spatial–frequency domain transformation for infrared small target detection. *IEEE Transactions on Geoscience and Remote Sensing*, 63:1–16, 2025b.
- Liu, Z., Liu, J., Wu, G., Ma, L., Fan, X., and Liu, R. Bi-level dynamic learning for jointly multi-modality image fusion and beyond. In *International Joint Conference on Artificial Intelligence*, pp. 1240–1248. IJCAI Press, 2023a.
- Liu, Z., Liu, J., Zhang, B., Ma, L., Fan, X., and Liu, R. PAIF: Perception-aware infrared-visible image fusion for attack-tolerant semantic segmentation. In *Proceedings of the 31st ACM International Conference on Multimedia*, pp. 3706–3714, 2023b.
- Liu, Z., Wang, Z., Liu, J., Meng, F., Ma, L., and Liu, R. DEAL: Data-efficient adversarial learning for high-quality infrared imaging. In *Proceedings of the IEEE/CVF Conference on Computer Vision and Pattern Recognition*, pp. 28198–28207, 2025c.
- Lu, X., Yue, T., Cai, J., Chen, Y., Lv, C., and Chu, S. MSCANet: Multi-scale context aggregation network for infrared small target detection. *Optics & Laser Technology*, 192: 113894, 2025.
- Lu, Y., Lin, Y., Wu, H., Xian, X., Shi, Y., and Lin, L. SIRST-5K: Exploring massive negatives synthesis with self-supervised learning for robust infrared small target detection. *IEEE Transactions on Geoscience and Remote Sensing*, 62:1–11, 2024.
- Luo, J., Yang, X., Yu, Y., Li, Q., Yan, J., and Li, Y. PointOBB: Learning oriented object detection via single point supervision. In *Proceedings of the IEEE/CVF Conference on Computer Vision and Pattern Recognition*, pp. 16730–16740, 2024.
- Metzger, N., Daudt, R. C., and Schindler, K. Guided depth super-resolution by deep anisotropic diffusion. In *Proceedings of the IEEE/CVF Conference on Computer Vision and Pattern Recognition*, pp. 18237–18246. IEEE, 2023.
- Ravi, N., Gabeur, V., Hu, Y.-T., Hu, R., Ryali, C., Ma, T., Khedr, H., Rädle, R., Rolland, C., Gustafson, L., et al. SAM 2: Segment anything in images and videos. In *International Conference on Learning Representations*, 2025.
- Wang, H., Zhou, L., and Wang, L. Miss detection vs. false alarm: Adversarial learning for small object segmentation in infrared images. In *Proceedings of the IEEE/CVF International Conference on Computer Vision*, pp. 8509–8518. IEEE, 2019.
- Wang, Y., Jin, D., Chen, J., and Bai, X. Revelation of hidden 2D atmospheric turbulence strength fields from turbulence effects in infrared imaging. *Nature Computational Science*, 3(8):687–699, 2023.
- Wang, Y., Zhao, J., Fan, Z., Zhang, X., Wu, X., Zhang, Y., Jin, L., Li, X., Wang, G., Jia, M., et al. JTD-UAV: MLLM-enhanced joint tracking and description framework for anti-UAV systems. In *Proceedings of the IEEE/CVF Conference on Computer Vision and Pattern Recognition*, pp. 1633–1644. IEEE, 2025.

- Wu, X., Hong, D., and Chanussot, J. UIU-Net: U-Net in U-Net for infrared small object detection. *IEEE Transactions on Image Processing*, 32:364–376, 2023.
- Xu, H., Zhong, S., Zhang, T., and Zou, X. Multiscale multilevel residual feature fusion for real-time infrared small target detection. *IEEE Transactions on Geoscience and Remote Sensing*, 61:1–16, 2023.
- Ying, X., Liu, L., Wang, Y., Li, R., Chen, N., Lin, Z., Sheng, W., and Zhou, S. Mapping degeneration meets label evolution: Learning infrared small target detection with single point supervision. In *Proceedings of the IEEE/CVF Conference on Computer Vision and Pattern Recognition*, pp. 15528–15538. IEEE, June 2023.
- Yu, C., Liu, Y., Wu, S., Hu, Z., Xia, X., Lan, D., and Liu, X. Infrared small target detection based on multiscale local contrast learning networks. *Infrared Physics & Technology*, 123:104107, 2022a.
- Yu, C., Liu, Y., Wu, S., Xia, X., Hu, Z., Lan, D., and Liu, X. Pay attention to local contrast learning networks for infrared small target detection. *IEEE Geoscience and Remote Sensing Letters*, 19:1–5, 2022b.
- Yu, C., Zhao, J., Liu, Y., Zhao, S., Dai, Y., and Yue, X. From easy to hard: Progressive active learning framework for infrared small target detection with single point supervision. In *Proceedings of the IEEE/CVF International Conference on Computer Vision*, pp. 2588–2598. IEEE, 2025a.
- Yu, Y., Ren, B., Zhang, P., Liu, M., Luo, J., Zhang, S., Da, F., Yan, J., and Yang, X. Point2RBox-v2: Rethinking point-supervised oriented object detection with spatial layout among instances. In *Proceedings of the Computer Vision and Pattern Recognition Conference*, pp. 19283–19293, 2025b.
- Yu, Y., Yang, X., Li, Y., Han, Z., Da, F., and Yan, J. Wholly-WOOD: Wholly leveraging diversified-quality labels for weakly-supervised oriented object detection. *IEEE Transactions on Pattern Analysis and Machine Intelligence*, 2025c.
- Zhang, M., Yue, K., Zhang, J., Li, Y., and Gao, X. Exploring feature compensation and cross-level correlation for infrared small target detection. In *Proceedings of the 30th ACM International Conference on Multimedia*, pp. 1857–1865. ACM, 2022a.
- Zhang, M., Zhang, R., Yang, Y., Bai, H., Zhang, J., and Guo, J. ISNet: Shape matters for infrared small target detection. In *Proceedings of the IEEE/CVF Conference on Computer Vision and Pattern Recognition*, pp. 877–886. IEEE, 2022b.
- Zhang, M., Wang, Y., Guo, J., Li, Y., Gao, X., and Zhang, J. IRSAM: Advancing segment anything model for infrared small target detection. In *European Conference on Computer Vision*, pp. 233–249. Springer, 2024a.
- Zhang, M., Zhang, C., Zhang, Q., Li, Y., Gao, X., and Zhang, J. Unleashing the power of generic segmentation model: A simple baseline for infrared small target detection. In *Proceedings of the 32nd ACM International Conference on Multimedia*, pp. 10392–10401. ACM, 2024b.
- Zhang, M., Li, X., Gao, F., Guo, J., Gao, X., and Zhang, J. SAIST: Segment any infrared small target model guided by contrastive language-image pretraining. In *Proceedings of the IEEE/CVF Conference on Computer Vision and Pattern Recognition*, pp. 9549–9558. IEEE, 2025a.
- Zhang, M., Shang, W., Gao, F., Zhang, Q., Lu, F., and Zhang, J. Semi-supervised infrared small target detection with thermodynamic-inspired uneven perturbation and confidence adaptation. In *Proceedings of the AAAI Conference on Artificial Intelligence*, volume 39, pp. 10013–10021. AAAI Press, 2025b.
- Zhao, J., Yu, C., Shi, Z., Liu, Y., and Zhang, Y. Gradient-guided learning network for infrared small target detection. *IEEE Geoscience and Remote Sensing Letters*, 20: 1–5, 2023.
- Zhao, J., Shi, Z., Yu, C., Liu, Y., Ying, X., and Dai, Y. Multi-scale direction-aware network for infrared small target detection. *IEEE Transactions on Geoscience and Remote Sensing*, 63:1–18, 2025.
- Zhao, M., Li, W., Li, L., Hu, J., Ma, P., and Tao, R. Single-frame infrared small-target detection: A survey. *IEEE Geoscience and Remote Sensing Magazine*, 10(2):87–119, 2022.
- Zhu, H., Liu, S., Deng, L., Li, Y., and Xiao, F. Infrared small target detection via low-rank tensor completion with top-hat regularization. *IEEE Transactions on Geoscience and Remote Sensing*, 58(2):1004–1016, 2020.